Post-Processing for Exoplanet Imaging with the Nancy Grace Roman Space Telescope Coronagraph Instrument

Author: Kenneth Casimiro (Jet Propulsion Laboratory, California Institute of Technology)

Primary Mentor: Dr. Marie Ygouf
Co-Mentor: Dr. Vanessa Bailey

ABSTRACT

The Coronagraph Instrument (CGI) on the Nancy Grace Roman Space Telescope will be capable of detecting and characterizing terrestrial planets in reflected light at an unprecedented contrast of $\sim 10^{-9}$ between a planet and its host star. This process is not perfect and stellar residuals prevent the planet signal from being detected. Therefore, innovative post-processing techniques are being developed to compensate for the instrument's limitation. This paper presents an overview of my project, methodology, results, and the conclusions of my findings under the mentorship and guidance of Dr. Marie Ygouf and Dr. Vanessa Bailey to develop post-processing tools in Python and perform tests on the most recent Roman CGI simulated data. My primary task was to show improvement of contrast by region selection by using an existing python framework to process simulated data with several post-processing techniques and compare their performance against a selected image region. I created several contrast gains plots as a function of separation for different regions used and post-processing techniques. In the end, I successfully made recommendations for specific image regions/masks to be used to optimize each post-processing technique's performance.

OVERVIEW

The Nancy Grace Roman Space Telescope will be using direct imaging to look at exoplanets. Direct imaging is a method of planet detection that takes an image of a planet next to its star. While solar systems planets are often the brightest objects in the night sky and therefore easily detected, planets around other stars are more difficult to directly detect. There are two primary reasons: they are faint, and they are located close proximity to their extremely bright host star. Therefore, the challenge of directly imaging a planet

comes down to the problem of separation of an extremely faint image of a planet from the extreme glare of its host star. That is where the Coronagraph Instrument (CGI) comes into play, it is there to block the light from the planet's host star, so we can find the surrounding planets from that starlight. The CGI is one of two instruments onboard the Nancy Grace Roman Space Telescope, which is expected to launch in 2026. The Roman CGI will be capable of detecting and characterizing exoplanets in reflected light at an unprecedented ratio of flux, or contrast, of $\sim 10^{-9}$ between a planet and its host star. As Roman CGI is a technology demonstrator, it will provide a crucial steppingstone in preparing future missions aiming to image and characterize exoplanets. The process of direct imaging observations takes up to a few to hundreds of hours to detect the faint signal from the planet. Although the CGI is blocking the starlight, there is still stellar residuals in the final image which prevents us to detect the planet. Therefore, post-processing is required, if we do not have post-processing then we are unable to detect those planets. As a result, innovative post-processing techniques are being developed to compensate for the instrument's limitation.

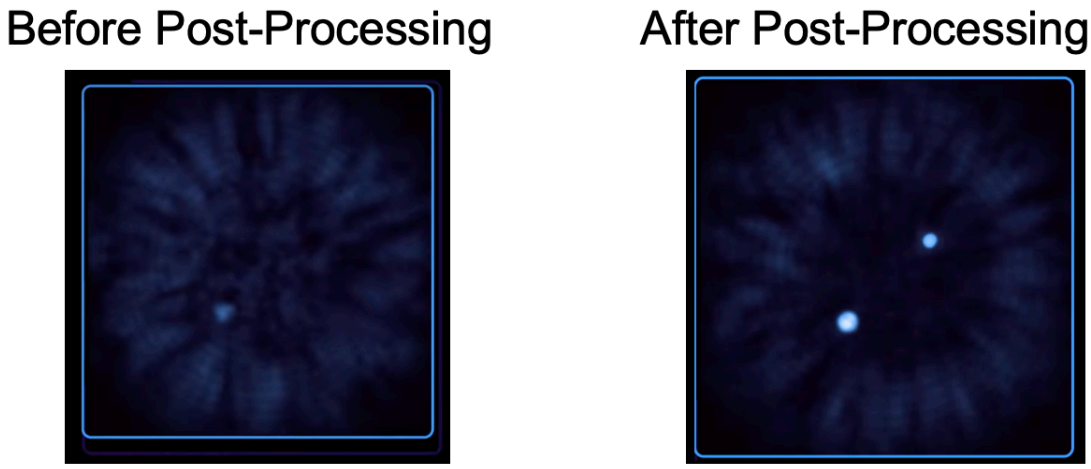

These images are for illustration purpose and are not realistic simulated images from the Roman CGI.

Figure 1: The left image is the final image without post-processing and the right image is the final image with post-processing. As you can see one faint planet in the left but by removing the stellar residuals, we can see that there were two planets in the image. Source: NASA Goddard: Coronagraph Instrument for Roman

During this internship, I improved optimization of the post-processing framework and performed tests on the most recent CGI simulated data. My primary task was to determine the optimal region of the image to be used for the optimization of post-processing techniques. I created several contrast gains plots as a function of separation for different regions used and techniques of post-processing. For the end of the project, I

made a table of recommendations for specific image regions/masks to be used in order to optimize the performance of each post-processing technique. Therefore, by optimizing the framework developed by my mentor, Dr. Marie Ygouf, and Neil Zimmerman from NASA Goddard, I discovered the relationships of improved contrast with each post-processing technique and the different regions of the exoplanet image.

The datasets that I worked with are:

- Noiseless without planets with and without Model Uncertainty Factor (MUF)
- Noiseless with planets with and without MUF
- Noisy without planets with and without MUF
- Noisy with planets with and without MUF

These datasets were produced by John Krist and the integrated modeling team at JPL to create simulated CGI data for the Hybrid Lyot Coronagraph (HLC). The OS9 data uses a target star called 47 UMa and a reference star ζPup. The data represents the Roman CGI data as it was produced by the observing sequence simulated in OS9. These simulated were repeated to produce the eight different datasets above. Noiseless dataset has the residual speckles as the limiting factor while noisy dataset has the photon noise as the limiting factor. The unprocessed data sets that are available by the Observing Scenario (OS) 9 time series simulations for the Hybrid Lyot Coronagraph Band 1. The OS9 distribution is publicly available at the Infrared Processing and Analysis Center (IPAC) website for the Nancy Grace Roman Space Telescope.

The post-processing methods that I worked with and optimized the region of the image for are the following:

- Classical Point Spread Function (PSF) techniques
    - Classical Angular Differential Imaging (cADI), consisting of calibrating the stellar residuals by observing the target at different rolls angles (+/- 11°).
    - Classical Reference Star Differential Imaging (cRDI), consisting of observing a reference star to calibrate the stellar residuals.
- Principal Component Analysis (PCA)
    - KLIP, a technique that uses the reference cube as a library of reference point spread functions.

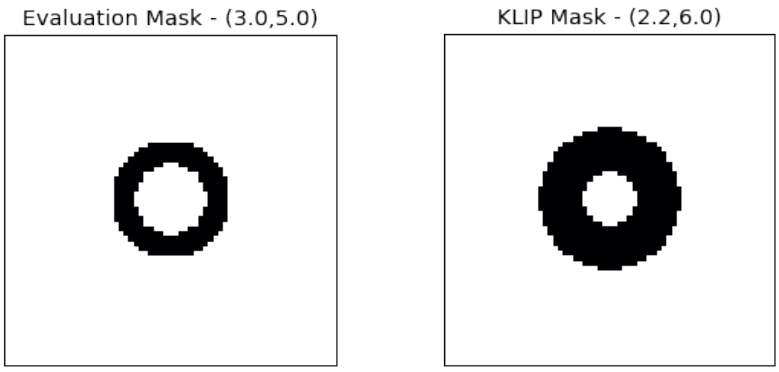

Figure 2: The two images is an example of the evaluation mask and the KLIP mask display. The evaluation mask is the region (pixels) that we are only taking into account. The inner angle and outer angle for each mask will be changed in this project to determine the optimal post-processing technique with the most improved contrast for each region. Their units being λ/D. λ being the wavelength and D being the diameter of the aperture.

Additionally, I was given the task to implement the cADI and the cRDI throughput correction; correcting how much of the planet light has been subtracted from the PSF subtraction.

METHODS

Data Visualization of Optimal Regions for Post-Processing Techniques

The primary method to display my findings and determining the relationship of improved contrast will be producing graphs in the Python framework. I used the post-processing code that utilizes cADI, cRDI, and KLIP to calculate the contrast of the image. I was able optimize this code to find the various regions that would improve contrast. I created iterations in the program for each run through of the dataset and plotted the contrast for each differing evaluation and KLIP mask on a graph for each post-processing technique. In the end, I presented my findings and analyzed the curves with my mentors to determine the trends/patterns of contrast to the different evaluation mask and KLIP mask used for each dataset.

I stored each post processing technique plot with respect to each dataset in their own list. At the start of the code, I made sure I can easily switch the evaluation mask for each test run. I implement two repetition structures that encapsulates the post-processing section of the code that increments the inner-working angle and the outer-working angle of the KLIP mask. I did three test cases with the inner angles going from 2.5, 2.75, and 3.0, with the outer angles going in the range from 6.0 – 7.25 with increments of .25. I chose these

cases because I required a difference between the two angles to be greater than 2.5 and the max outer angle for the code to work properly. This produced graphs that show the relationship between the increase of the outer-working angle of the KLIP mask (x-axis), and the contrast calculated for respective post-processing technique (y-axis, 5 σ sensitivity) using Matplotlib. The different colors of each line are a different post-processing technique: blue being cRDI, green being KLIP, and red being cADI. The shape of the lines is the different inner-working angle of the KLIP mask: solid being an inner-working angle of 2.5, dashed being 2.75, and dotted being 3.0.

After optimizing the code, we result in a graph with all of the plotted contrast from the different KLIP mask configurations and the specified evaluation mask region. Therefore, we are able to determine the best post-processing technique for this region and determine the optimal mask. In summary, we are looking at the plot of the detection limits for each one of these post-processing methods, where the y-axis is showing the detection limit and the x axis showing the size of the optimization region. Additionally, when reading these graphs, the higher the contrast is worse and having a lower contrast is best. We want the 5 σ sensitivity to be smaller.

In *Figure 3* below, we can see that cADI with an inner-working angle of 3.0 and an outer-working angle of 7.25 results in the most improved contrast. Therefore, I would that having a larger separation between the two angles for the KLIP mask will result in the most improved contrast for a region of 5 — 7 λ/D.

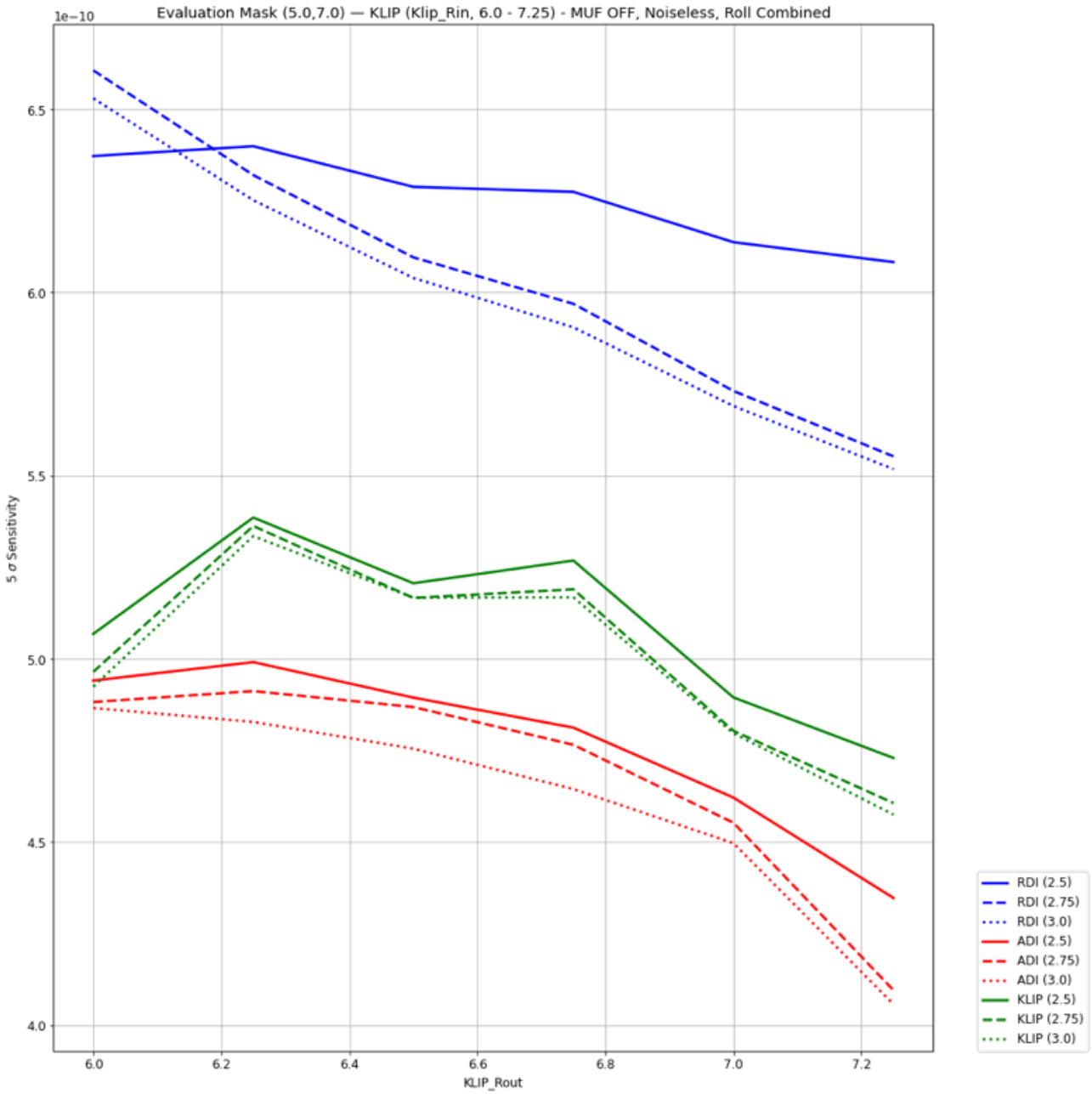

Figure 3: This graph uses an evaluation mask of $5 — 7\ \lambda/D$ for the MUF off, noiseless dataset. The graph shows the relationship between the increase of the outer angle of the KLIP mask (x-axis), and the contrast calculated for respective post-processing technique (y-axis, 5 σ sensitivity). The different colors of each line are a different post-processing technique, and the shape of the lines are the different inner-working angle of the KLIP mask.

cADI and cRDI Throughput Correction Implementation

Throughput correction is correcting how much of the planet light has been subtracted from the Point Spread Function (PSF) subtraction. To finalize my findings and analysis

of the most optimal regions for the post-processing techniques then the throughput correction for cADI and cRDI must be implemented. Currently in the code, KLIP throughput correction has been implemented. In *Figure 5*, you can see how I attempted to implement throughput correction with creating a set of fake planets and injecting them to the scene with the host star.

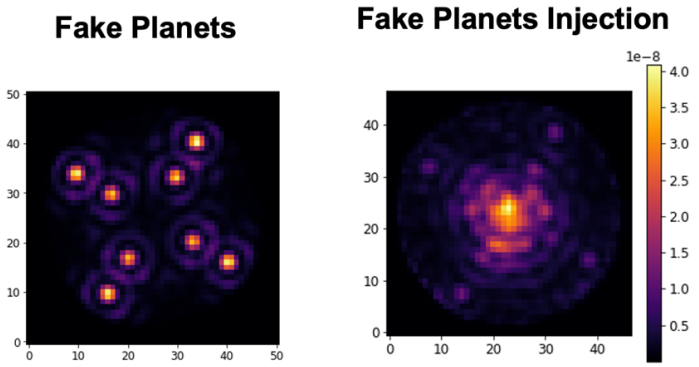

Figure 4: The left image shows where I determined the area to inject the fake planets and the right image shows the scene with the host star and the injected planets.

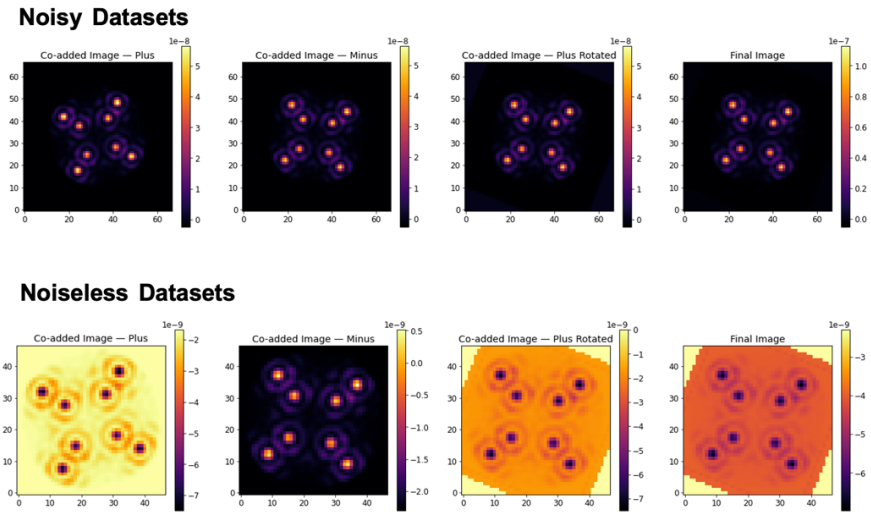

Figure 5: Creating the final image to be used to implement the throughput correction for cADI and cRDI. We can see that it is perfectly fine for noisy datasets, but it is showing negative contrast for noiseless datasets.

As we can see, at this part of the throughput correction implementation, that it is working perfectly fine for noisy datasets but as we start applying it to the noiseless datasets, the images are showing negative contrast. I was unable to understand and determine the reason why this is happening. This requires further investigation to finalize the project of determining the optimal regions for each post-processing technique.

RESULTS

Results — Recommendations for Optimal Regions.

	MUF OFF, Noiseless	MUF OFF, Noisy	MUF ON, Noiseless	MUF ON, Noisy
cADI	**3 — 4 λ/D**	**5 — 6 λ/D**	**5 — 6 λ/D**	**5 — 6 λ/D**
cRDI	**5 — 6 λ/D**	**4 — 5 λ/D**	**5 — 6 λ/D**	**5 — 6 λ/D**
RDI-KLIP	**4 — 5 λ/D**	**4 — 5 λ/D**	**5 — 6 λ/D**	**5 — 6 λ/D**

Figure 6: Table of optimal regions for each post-processing technique. The green filled boxes are the most optimal post-processing technique in each dataset.

After analyzing my graphs, I was able to create the table in *Figure 6* showcasing the optimal evaluation mask configurations for each post-processing technique. I first noticed that the majority of the most improved contrast came from 4 — 5 λ/D and 5 — 6 λ/D. The consensus from all of these results is that typically the optimal region of 5 — 6 λ/D works well with MUF ON cases with the additional speckle noise. Furthermore, we can see that an optimal region closer to the center of the image performs best for MUF OFF cases. For the blocks that are green, it's an indicator to show that specific post-processing technique performs the best and results in the most improved contrast in the dataset. We can see that regardless of the MUF's, cADI excels in noiseless cases and cRDI and RDI-KLIP excels in noisy cases. This confirms that cADI is more stable than cRDI and RDI-KLIP in noiseless as noiseless data is more speckle dominated rather than shot noise dominated. cRDI and RDI-KLIP performs best in noisy cases as it is dominated with a combination of photon and detector noise rather than speckle. The order of which is best for RDI and RDI-KLIP might change when throughput correction has been implemented for RDI as currently, they are almost overlapping each other in certain datasets. Therefore, to finalize my analysis and project, throughput correction must be implemented.

CONCLUSIONS

In conclusion of my internship, I was able to implement the visualization of the data to show the optimal region for each dataset and post-processing technique. We were able to see that the majority of the most improved contrast came from an evaluation mask of 4 — 5 λ/D and 5 — 6 λ/D. Additionally, I was able to confirm the behavior of Classical Angular Differential Imaging (cADI), Classical Reference Star Differential Imaging (cRDI), and KLIP in noisy and noiseless datasets. Being that cADI is more stable in noiseless as it is more speckle dominated while cRDI and KLIP outperforms cADI in noisy as it is photon noise dominated. Although I was unable to complete the throughput correction for cADI and cRDI, my recommendation to continue the project would be to investigate the noiseless datasets to find out why they are producing negative contrast. The next step for investigation for implementing throughput would be to compare the flux of the injected planets to the flux of the injected planets after subtraction in order to understand the flux loss from the PSF subtraction. Since we are observing the target and the reference star and doing a subtraction of the reference star from the target to subtract the residual starlight, we may subtract some of the planet flux because the instrument is not perfectly stable between the observation of the target and reference star. Therefore, the next step is to estimate what is the impact of the post-processing on the planet itself. If we can measure the flux of the injected planes before the subtraction in the image and compare to the injected planet flux after linear regression, we can then evaluate the processing on the planet flux itself.

REFERENCES

1. Ygouf, Zimmerman, Bailey, Krist, Zellem, & Debes. (2021, April). Roman Coronagraph Instrument Post Processing Report - OS9 HLC Distribution. https://roman.ipac.caltech.edu/docs/sims/20210402_Roman_CGI_post_processing_report_URS.pdf

2. University of San Francisco, College of Arts and Sciences, Jet Propulsion Laboratory - California Institute of Technology, University of Alabama, NASA Goddard Space Flight Center, The SETI Institute, Space Telescope Science Institute, Steward Observatory, BAER Institute/NASA Ames Research Center, Kasdin, Bailey, Menneson, Zellem, Ygouf, Rhodes, Luchik, Zhao, Riggs, Seo, Krist, . . . Lupu. (2020, December). The Nancy Grace Roman Space Telescope Coronagraph Instrument (CGI) Technology Demonstration. N. Jeremy Kasdin.

3. NASA Jet Propulsion Laboratory. (2021). The Nancy Grace Roman Space Telescope. https://www.jpl.nasa.gov/missions/the-nancy-grace-roman-space-telescope

4. NASA Jet Propulsion Laboratory. (2021b). The Search for Alien Planets - How Coronagraphs Find Hidden Planets. https://exoplanets.nasa.gov/exep/coronagraphvideo/

5. Jet Propulsion Laboratory, California Institute of Technology, NASA Goddard Space Flight Center, Ygouf, M. Y., Zimmerman, N. Z., Bailey, V. B., Zellem, R. Z., Mennesson, B. M., Rhodes, J. R., & Hildebrandt, S. H. (2021). Demonstrating Exoplanet Detection and Characterization at Unprecedented Contrast Levels with the Roman Space Telescope Coronagraph Instrument. American Astronomical Society. https://aas237-aas.ipostersessions.com/default.aspx?s=D3-BF-7C-A9-0D-F1-1E-B2-07-0B-7C-C3-2E-5D-BC-3C&guestview=true

6. Space Telescope Science Institute. (n.d.). Roman Space Telescope. Retrieved May 24, 2021, from https://www.stsci.edu/roman

7. Nancy Grace Roman Space Telescope. (n.d.). NASA Goddard Space Flight Center. Retrieved May 24, 2021, from https://roman.gsfc.nasa.gov/observatory.html

8. Roman Space Telescope at IPAC. (n.d.). Infrared Processing and Analysis Center. Retrieved May 24, 2021, from https://roman.ipac.caltech.edu

ACKNOWLEDGEMENTS

The research was carried out at the Jet Propulsion Laboratory, California Institute of Technology, under a contract with the National Aeronautics and Space Administration (80NM0018D0004).

The work described here was carried out under an internship program administered through the JPL Education Office managed by Jenny Tieu and Jessica Parker for academic credit at Saddleback College.

Mentorship and guidance were given by Dr. Marie Ygouf as my primary mentor, Dr. Vanessa Bailey as my co-mentor, and the Roman CGI Science Team.

APPENDIX

The following are the plots that I made during this internship. I analyzed these graphs to determine the best region for optimization for the post-processing techniques.

Each graph will use a different evaluation mask and will be used with four different datasets:

- MUF OFF, Noiseless
- MUF OFF, Noisy
- MUF ON, Noiseless
- MUF ON, Noisy

The evaluation masks that I used are:

- 3 — 5 λ/D, *Figures 7 to 10*
- 5 — 7 λ/D, *Figures 11 to 14*
- 3 — 4 λ/D, *Figures 15 to 18*
- 4 — 5 λ/D, *Figures 19 to 22*
- 5 — 6 λ/D, *Figures 23 to 26*

The graphs show the relationship between the increase of the outer angle of the KLIP mask (x-axis), and the contrast calculated for respective post-processing technique (y-axis, 5 σ sensitivity). The different colors of each line are a different post-processing technique; red being Classical Angular Differential Imaging (cADI), blue being Classical Reference Star Differential Imaging (cRDI), and green being RDI-KLIP. The shape of the lines are the different inner-working angle of the KLIP mask with solid being 2.5 being solid, 2.75 being dashed, and 3.0 being dotted.

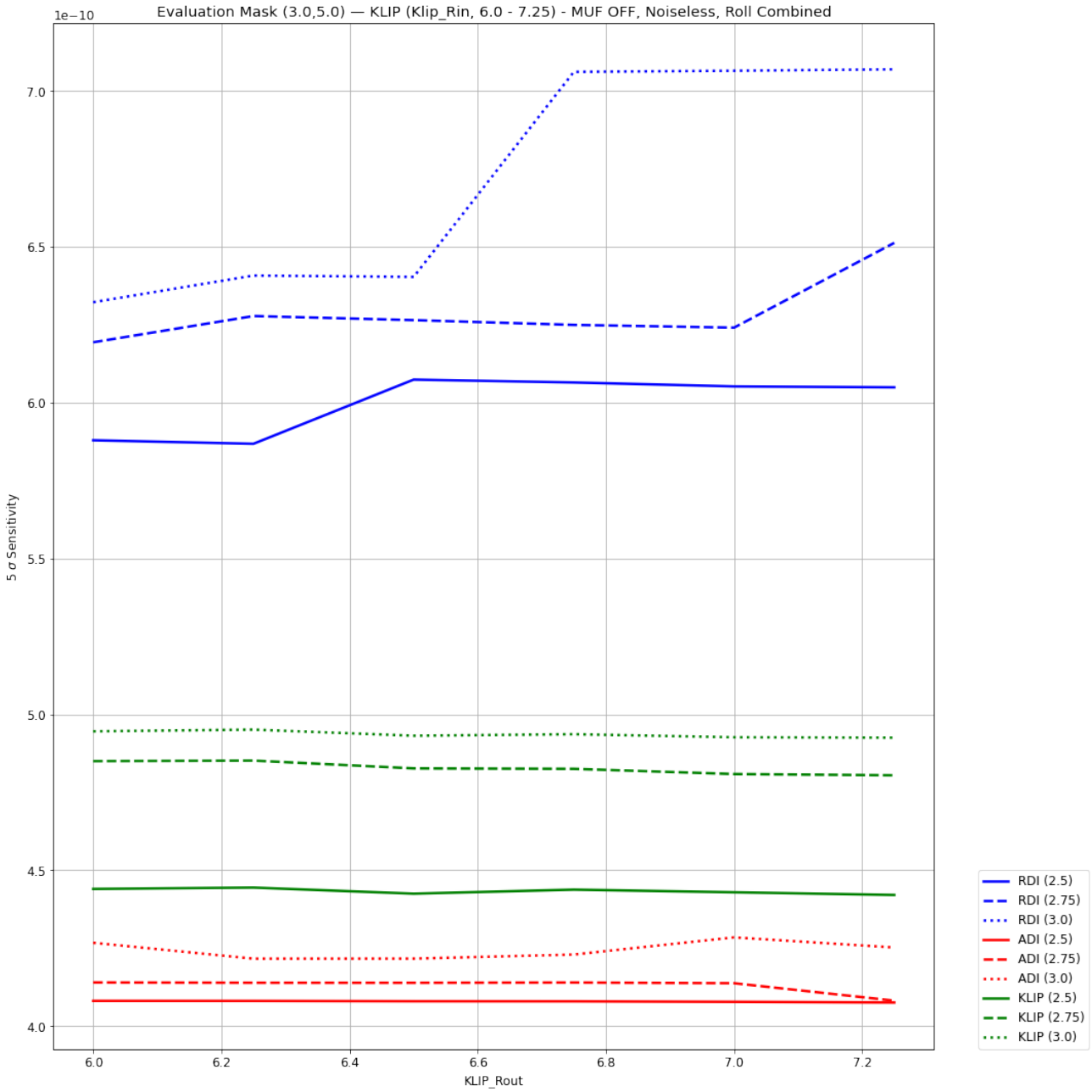

Figure 7: This graph uses an evaluation mask of 3 — 5 λ/D for the MUF off, noiseless dataset. The graph shows the relationship between the increase of the outer angle of the KLIP mask (x-axis), and the contrast calculated for respective post-processing technique (y-axis, 5 σ sensitivity). The different colors of each line are a different post-processing technique, and the shape of the lines are the different inner-working angle of the KLIP mask.

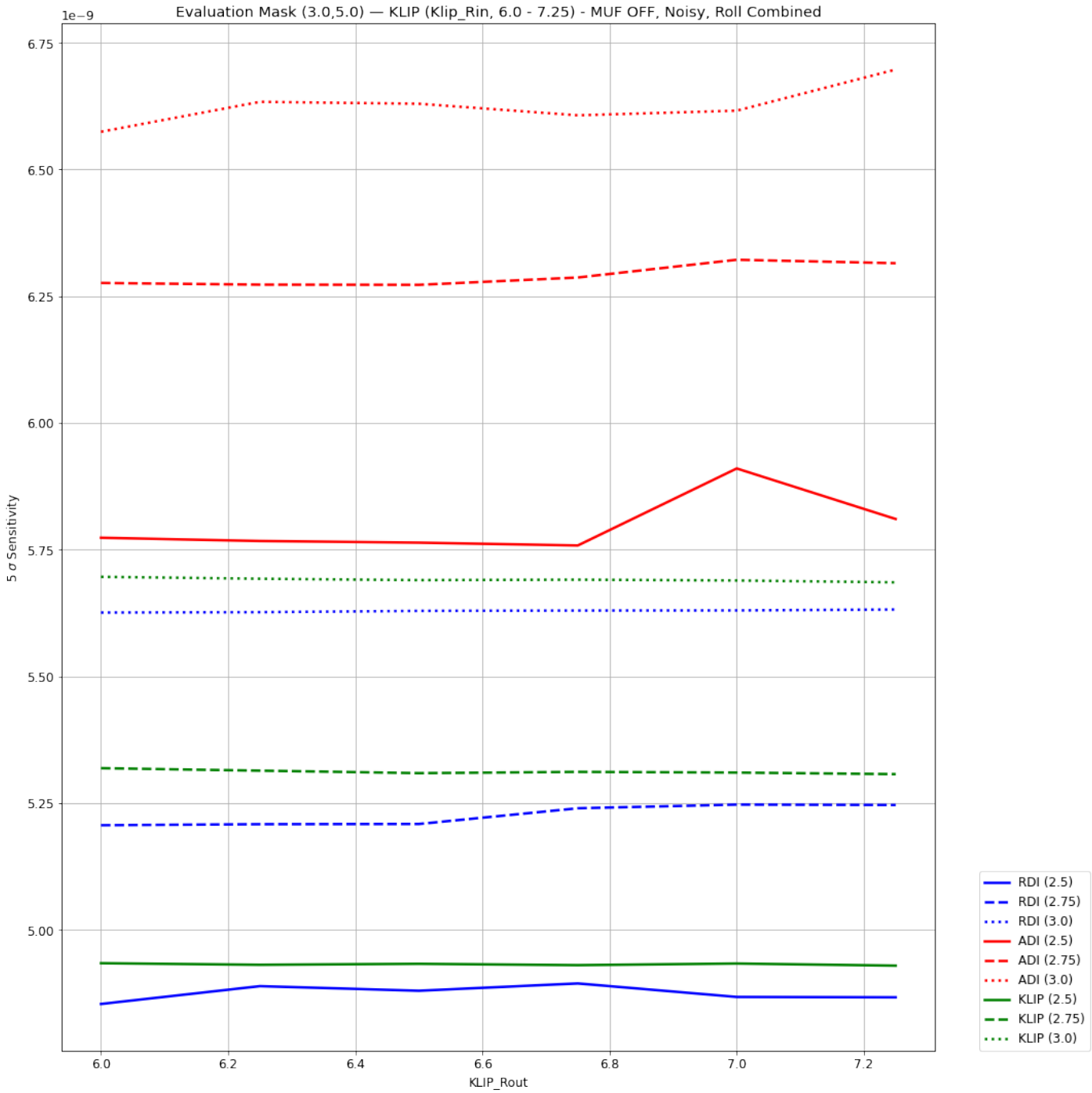

Figure 8: This graph uses an evaluation mask of 3 — 5 λ/D for the MUF off, noisy dataset. The graph shows the relationship between the increase of the outer angle of the KLIP mask (x-axis), and the contrast calculated for respective post-processing technique (y-axis, 5 σ sensitivity). The different colors of each line are a different post-processing technique, and the shape of the lines are the different inner-working angle of the KLIP mask.

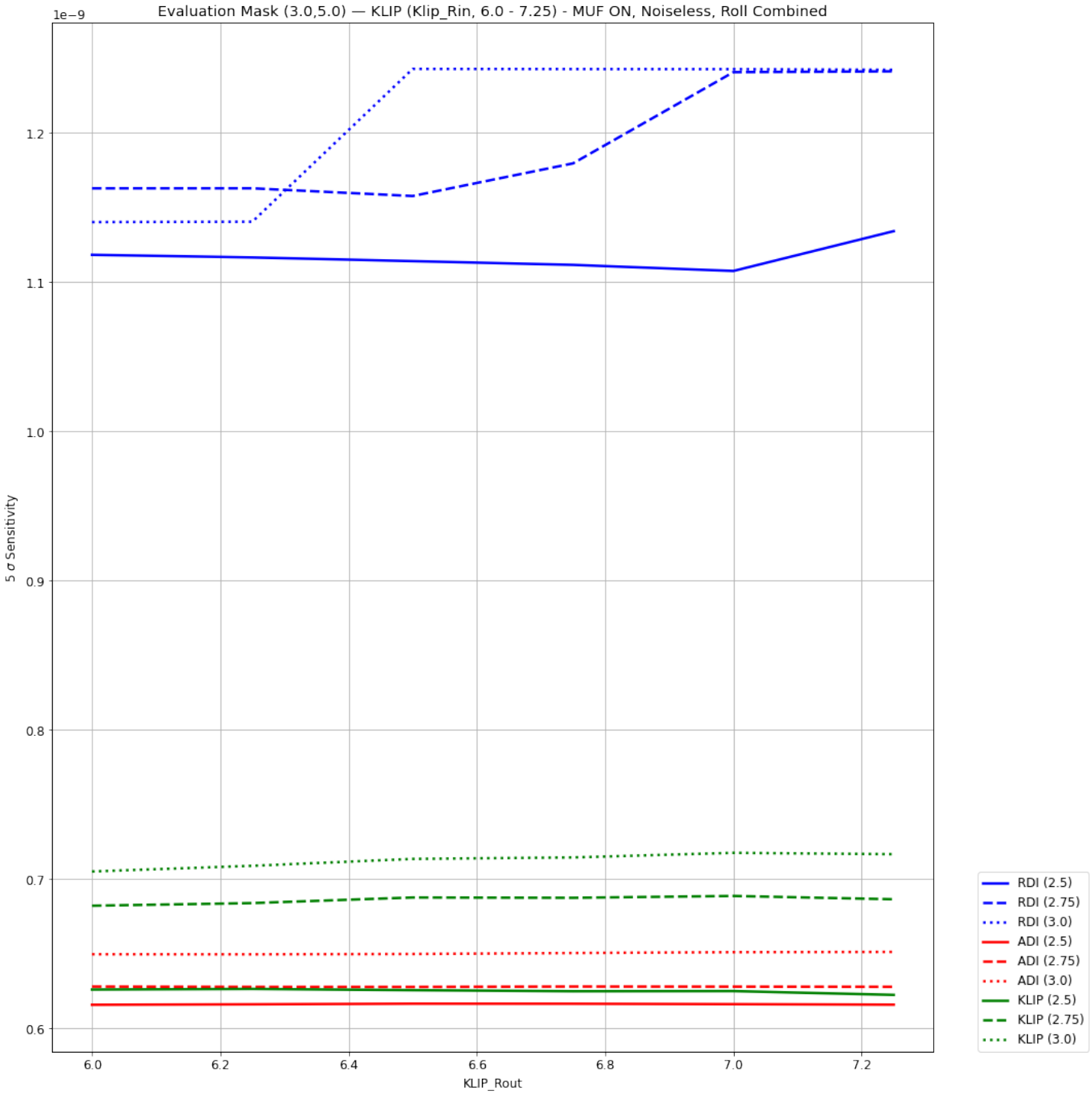

Figure 9: This graph uses an evaluation mask of 3 — 5 λ/D for the MUF on, noiseless dataset. The graph shows the relationship between the increase of the outer angle of the KLIP mask (x-axis), and the contrast calculated for respective post-processing technique (y-axis, 5 σ sensitivity). The different colors of each line are a different post-processing technique, and the shape of the lines are the different inner-working angle of the KLIP mask.

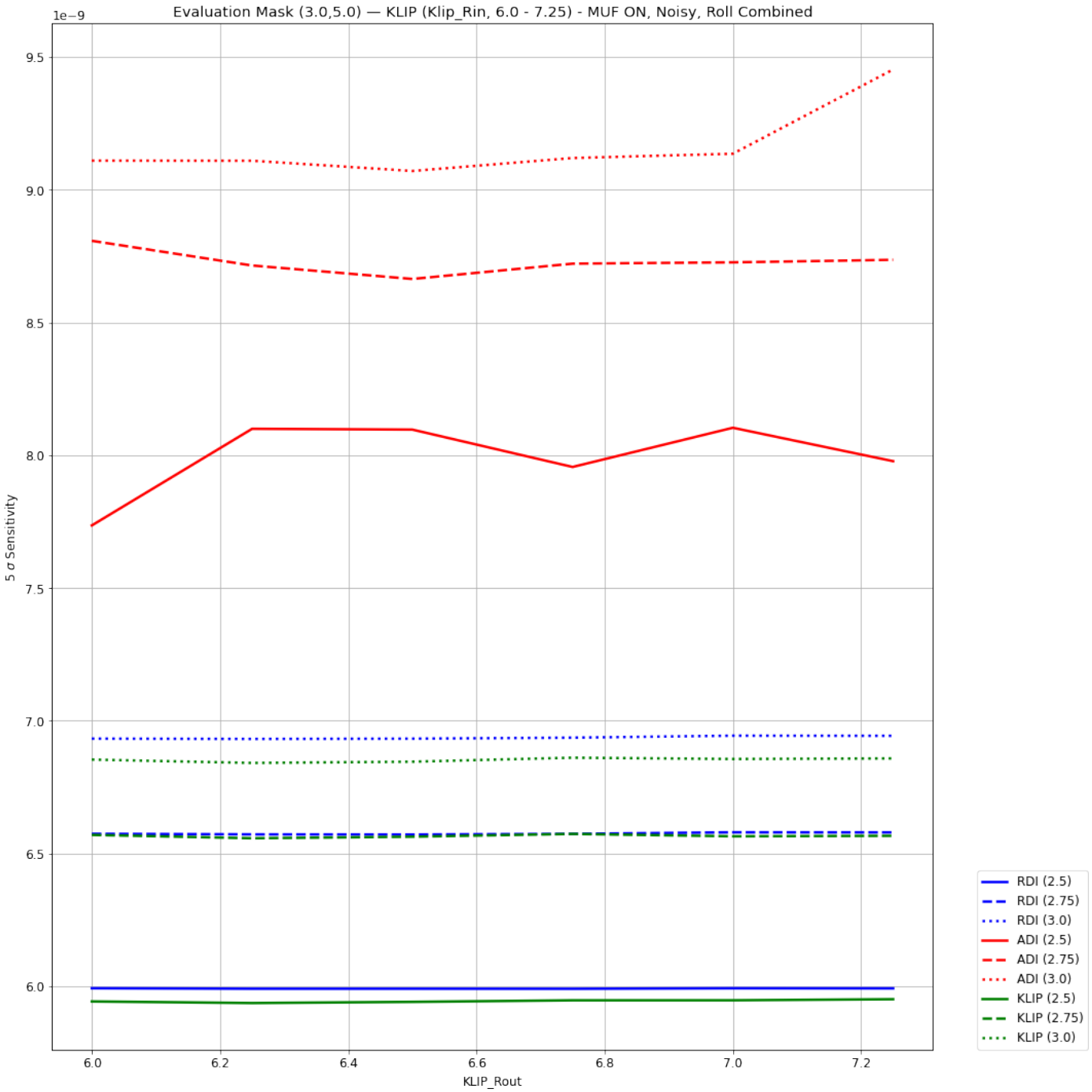

Figure 10: This graph uses an evaluation mask of 3 — 5 λ/D for the MUF on, noisy dataset. The graph shows the relationship between the increase of the outer angle of the KLIP mask (x-axis), and the contrast calculated for respective post-processing technique (y-axis, 5 σ sensitivity). The different colors of each line are a different post-processing technique, and the shape of the lines are the different inner-working angle of the KLIP mask.

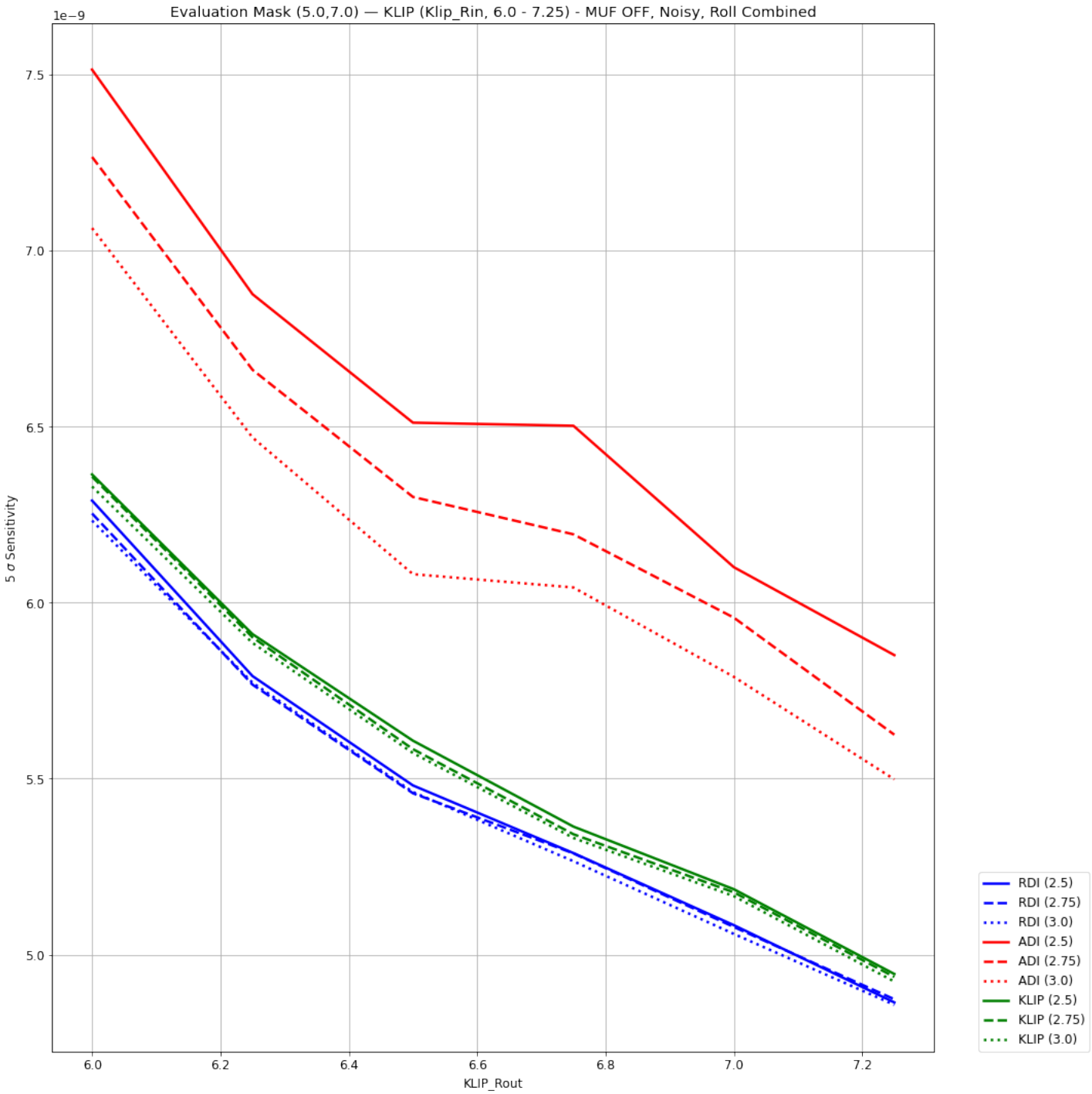

Figure 11: This graph uses an evaluation mask of 5 — 7 λ/D for the MUF off, noisy dataset. The graph shows the relationship between the increase of the outer angle of the KLIP mask (x-axis), and the contrast calculated for respective post-processing technique (y-axis, 5 σ sensitivity). The different colors of each line are a different post-processing technique, and the shape of the lines are the different inner-working angle of the KLIP mask.

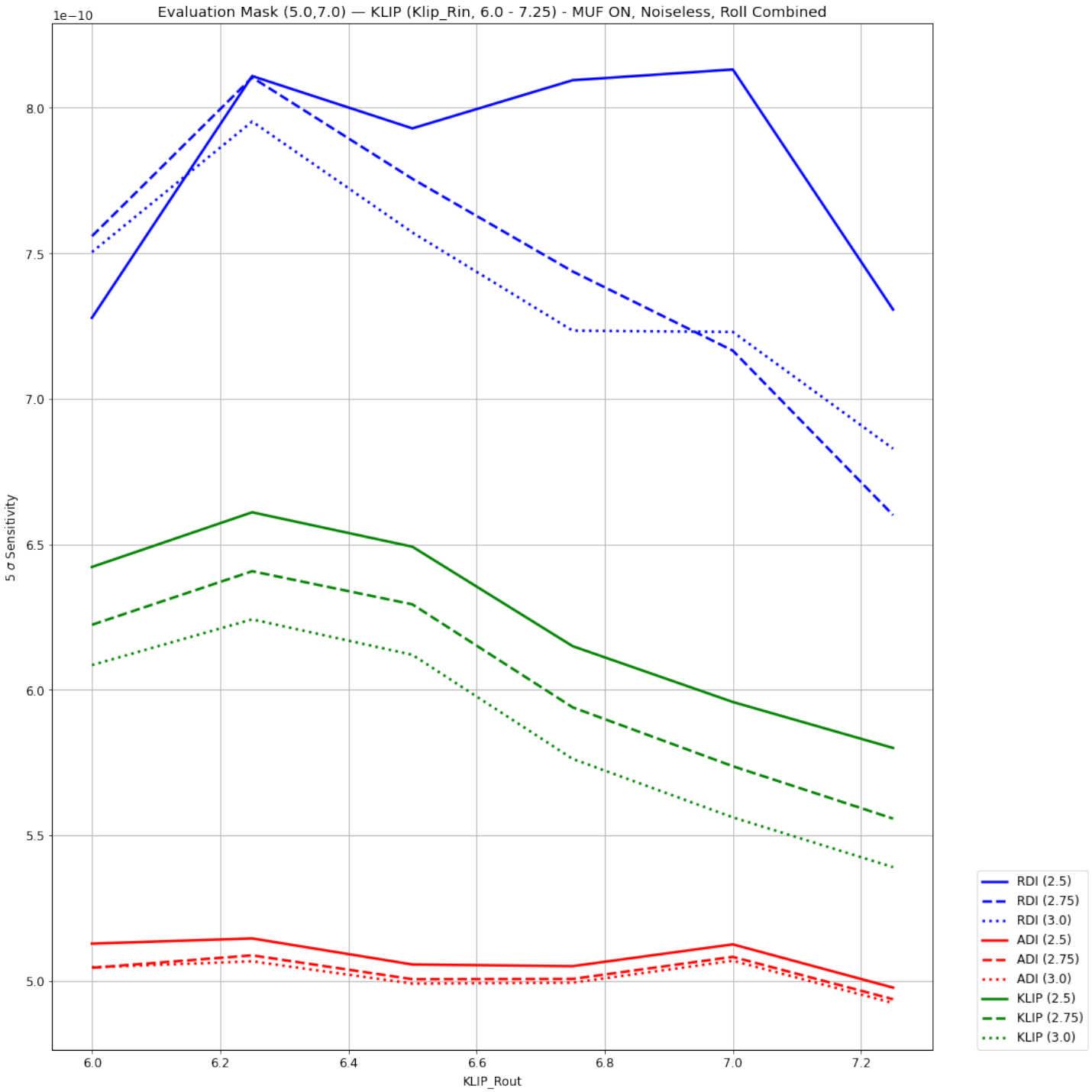

Figure 12: This graph uses an evaluation mask of $5 — 7\ \lambda/D$ for the MUF on, noiseless dataset. The graph shows the relationship between the increase of the outer angle of the KLIP mask (x-axis), and the contrast calculated for respective post-processing technique (y-axis, 5 σ sensitivity). The different colors of each line are a different post-processing technique, and the shape of the lines are the different inner-working angle of the KLIP mask.

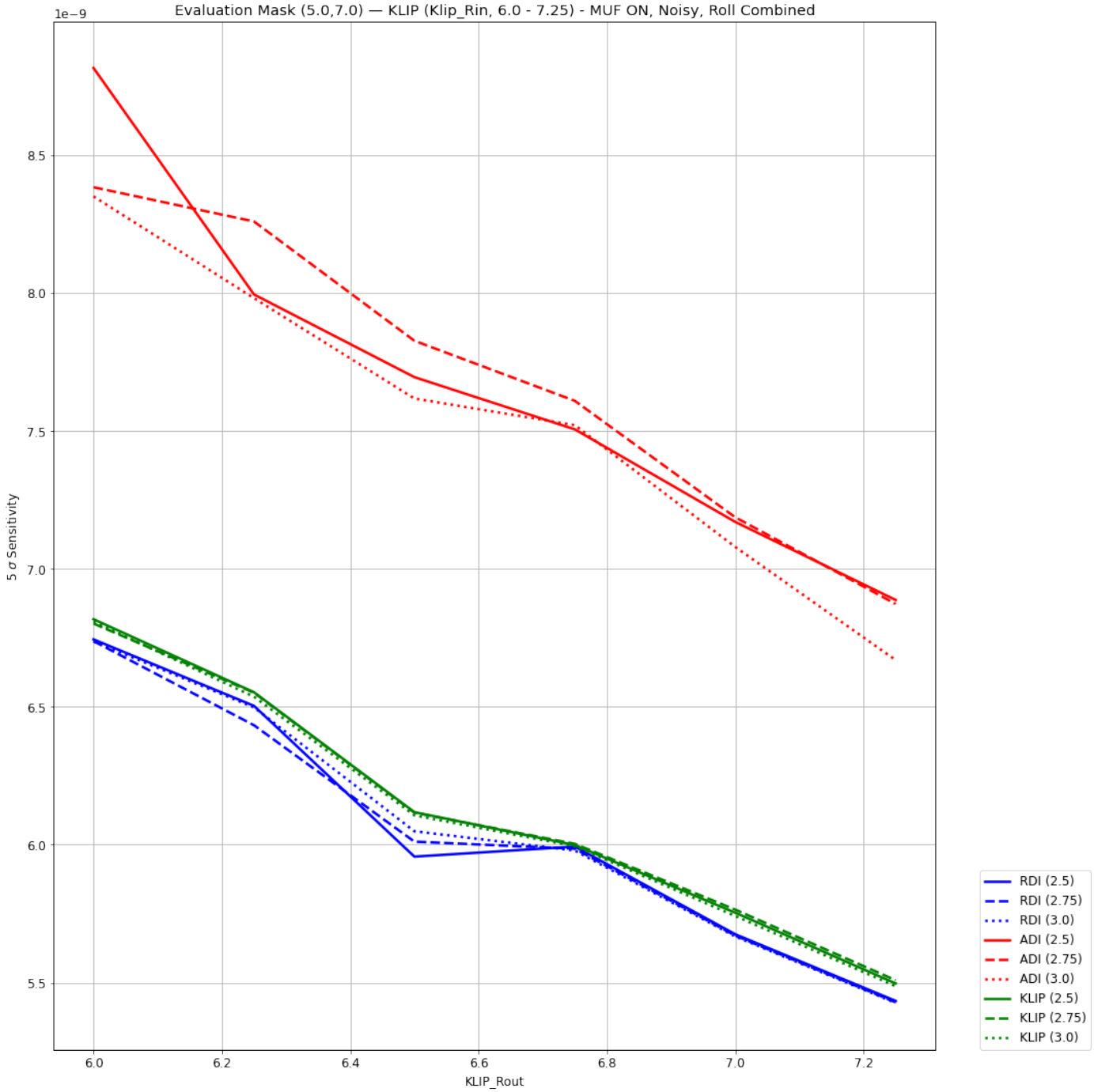

Figure 13: This graph uses an evaluation mask of 5 — 7 λ/D for the MUF on, noisy dataset. The graph shows the relationship between the increase of the outer angle of the KLIP mask (x-axis), and the contrast calculated for respective post-processing technique (y-axis, 5 σ sensitivity). The different colors of each line are a different post-processing technique, and the shape of the lines are the different inner-working angle of the KLIP mask.

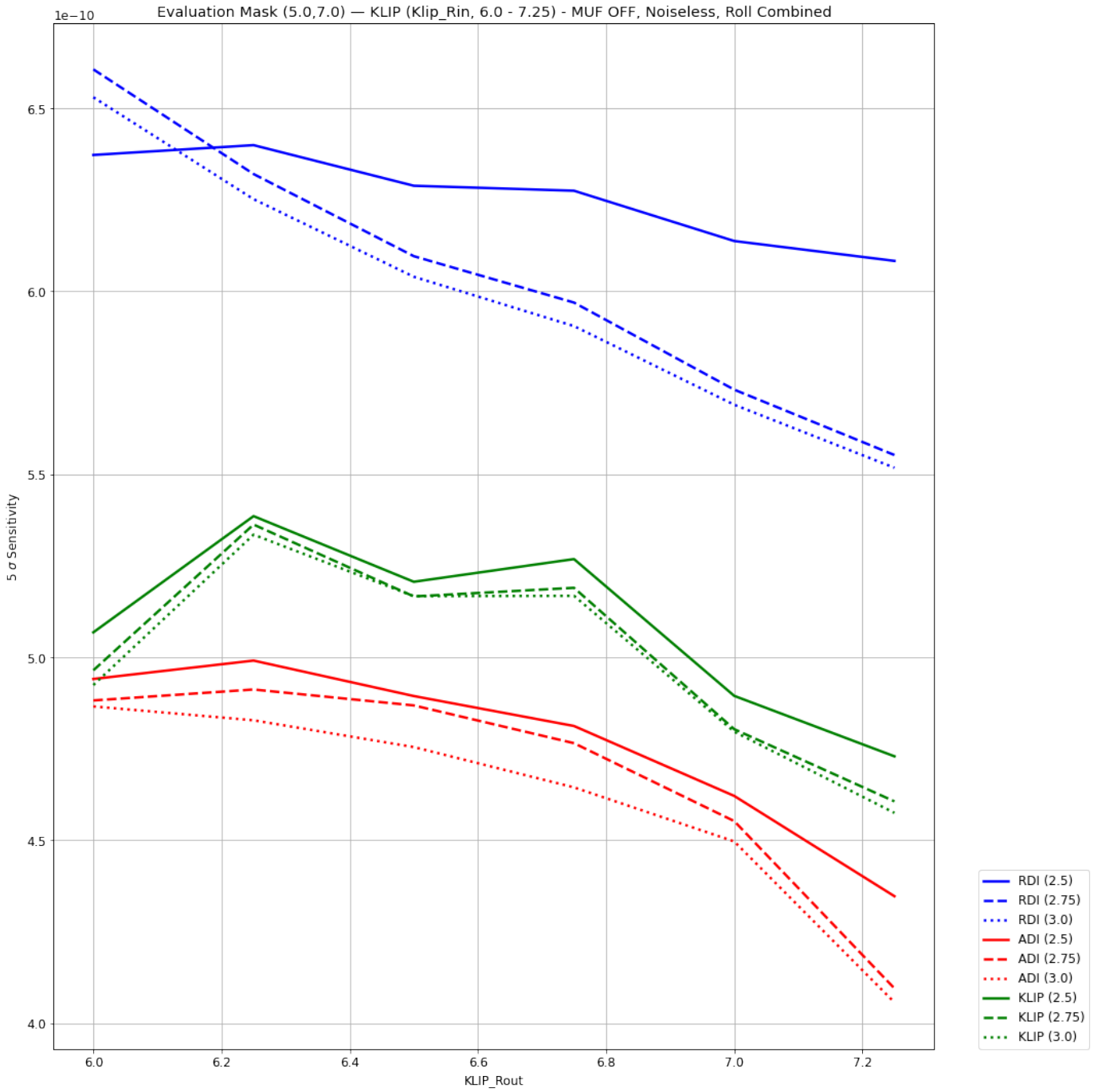

Figure 14: This graph uses an evaluation mask of 5 — 7 λ/D for the MUF off, noiseless dataset. The graph shows the relationship between the increase of the outer angle of the KLIP mask (x-axis), and the contrast calculated for respective post-processing technique (y-axis, 5 σ sensitivity). The different colors of each line are a different post-processing technique, and the shape of the lines are the different inner-working angle of the KLIP mask.

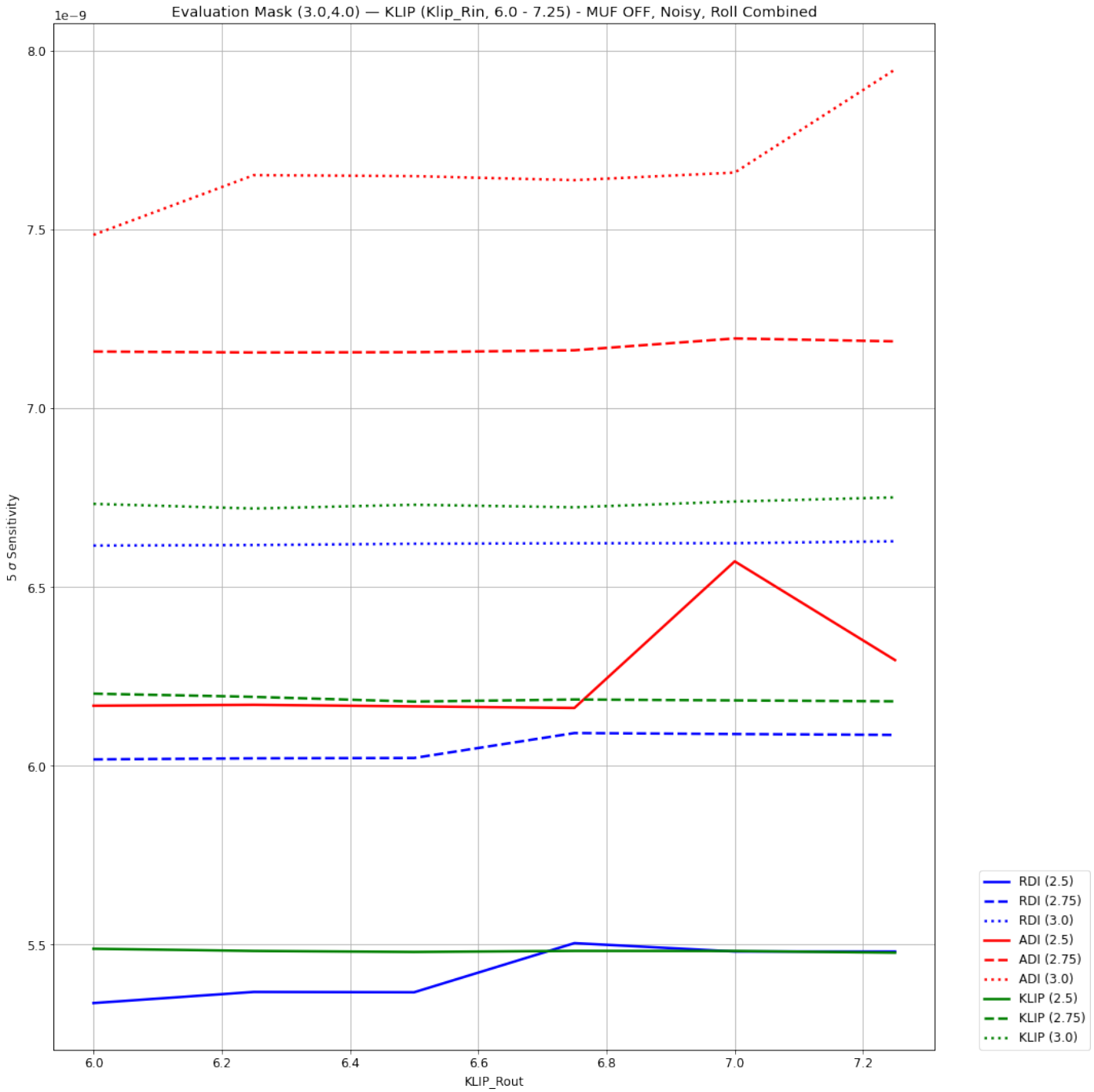

Figure 15: This graph uses an evaluation mask of 3 — 4 λ/D for the MUF off, noisy dataset. The graph shows the relationship between the increase of the outer angle of the KLIP mask (x-axis), and the contrast calculated for respective post-processing technique (y-axis, 5 σ sensitivity). The different colors of each line are a different post-processing technique, and the shape of the lines are the different inner-working angle of the KLIP mask.

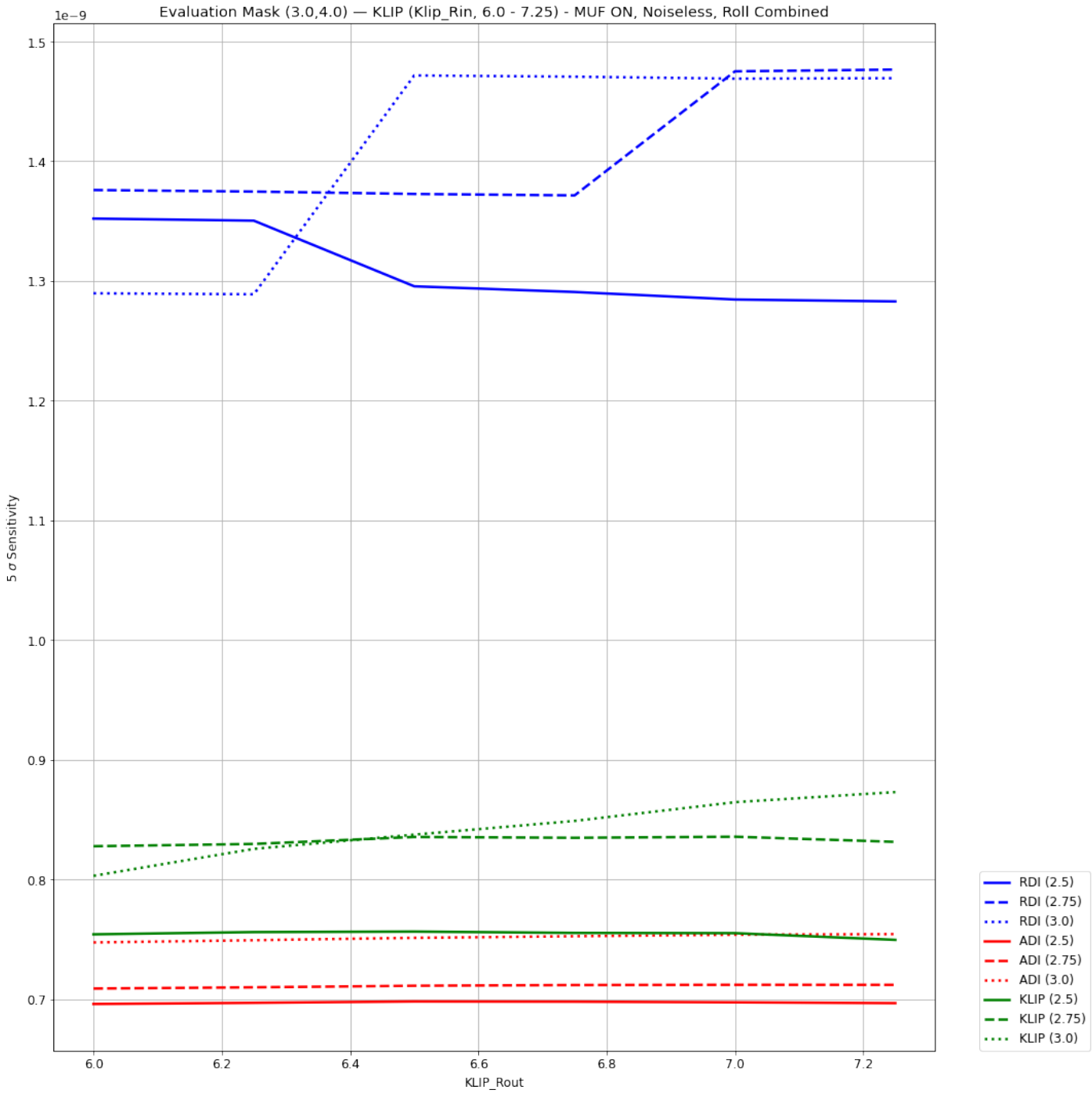

Figure 16: This graph uses an evaluation mask of 3 — 4 λ/D for the MUF on, noiseless dataset. The graph shows the relationship between the increase of the outer angle of the KLIP mask (x-axis), and the contrast calculated for respective post-processing technique (y-axis, 5 σ sensitivity). The different colors of each line are a different post-processing technique, and the shape of the lines are the different inner-working angle of the KLIP mask.

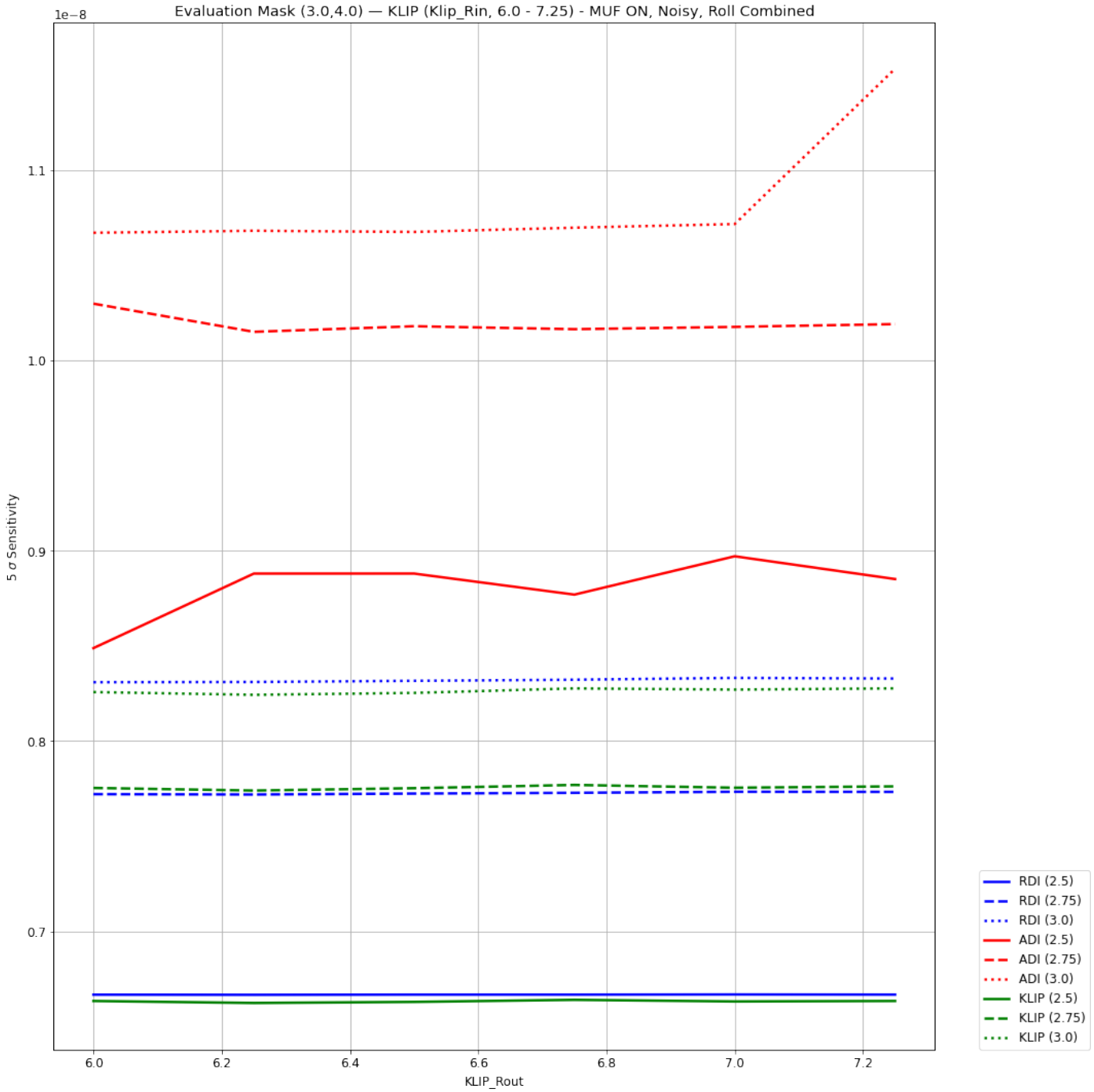

Figure 17: This graph uses an evaluation mask of 3 — 4 λ/D for the MUF on, noisy dataset. The graph shows the relationship between the increase of the outer angle of the KLIP mask (x-axis), and the contrast calculated for respective post-processing technique (y-axis, 5 σ sensitivity). The different colors of each line are a different post-processing technique, and the shape of the lines are the different inner-working angle of the KLIP mask.

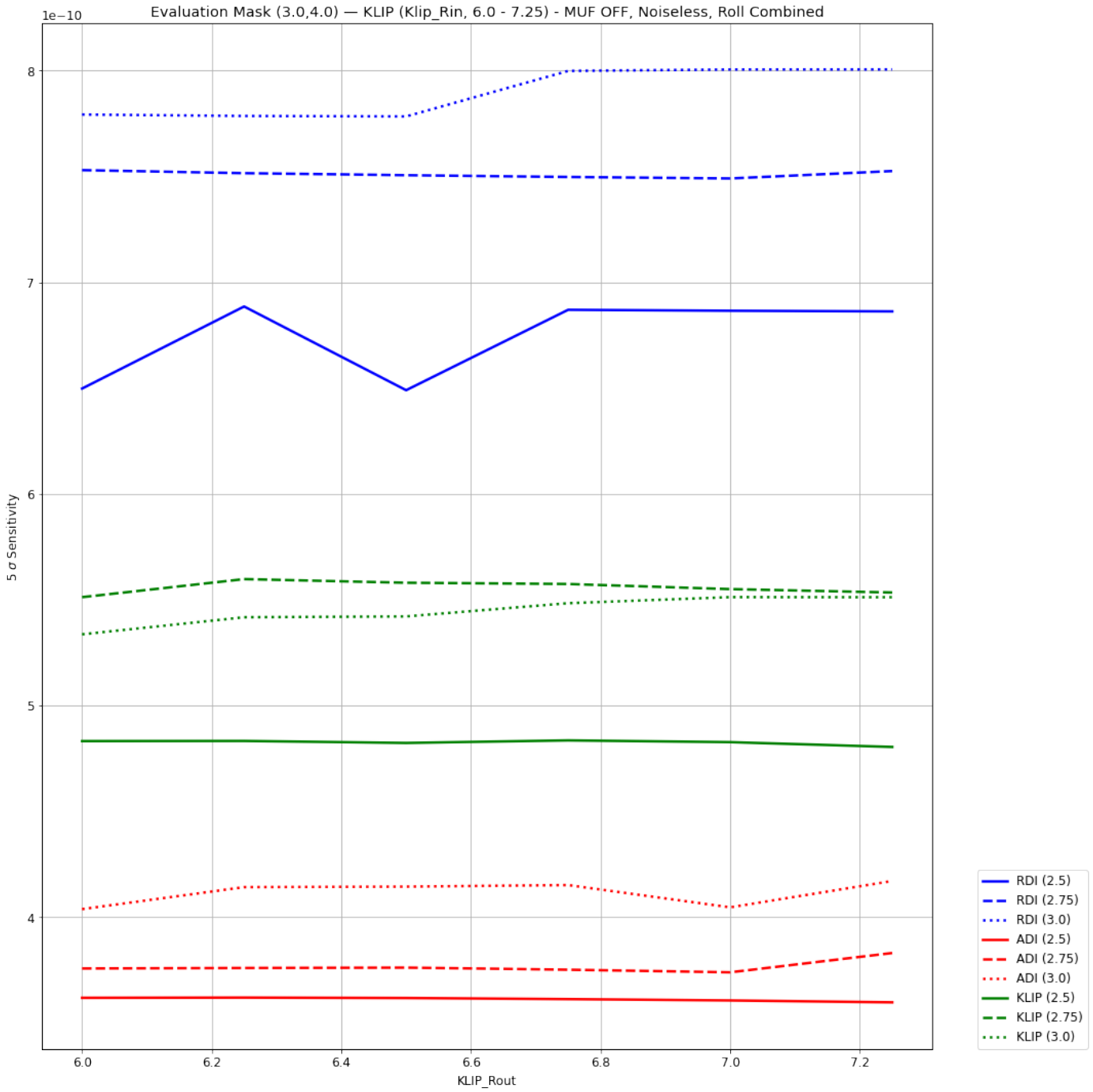

Figure 18: This graph uses an evaluation mask of 3 — 4 λ/D for the MUF off, noiseless dataset. The graph shows the relationship between the increase of the outer angle of the KLIP mask (x-axis), and the contrast calculated for respective post-processing technique (y-axis, 5 σ sensitivity). The different colors of each line are a different post-processing technique, and the shape of the lines are the different inner-working angle of the KLIP mask.

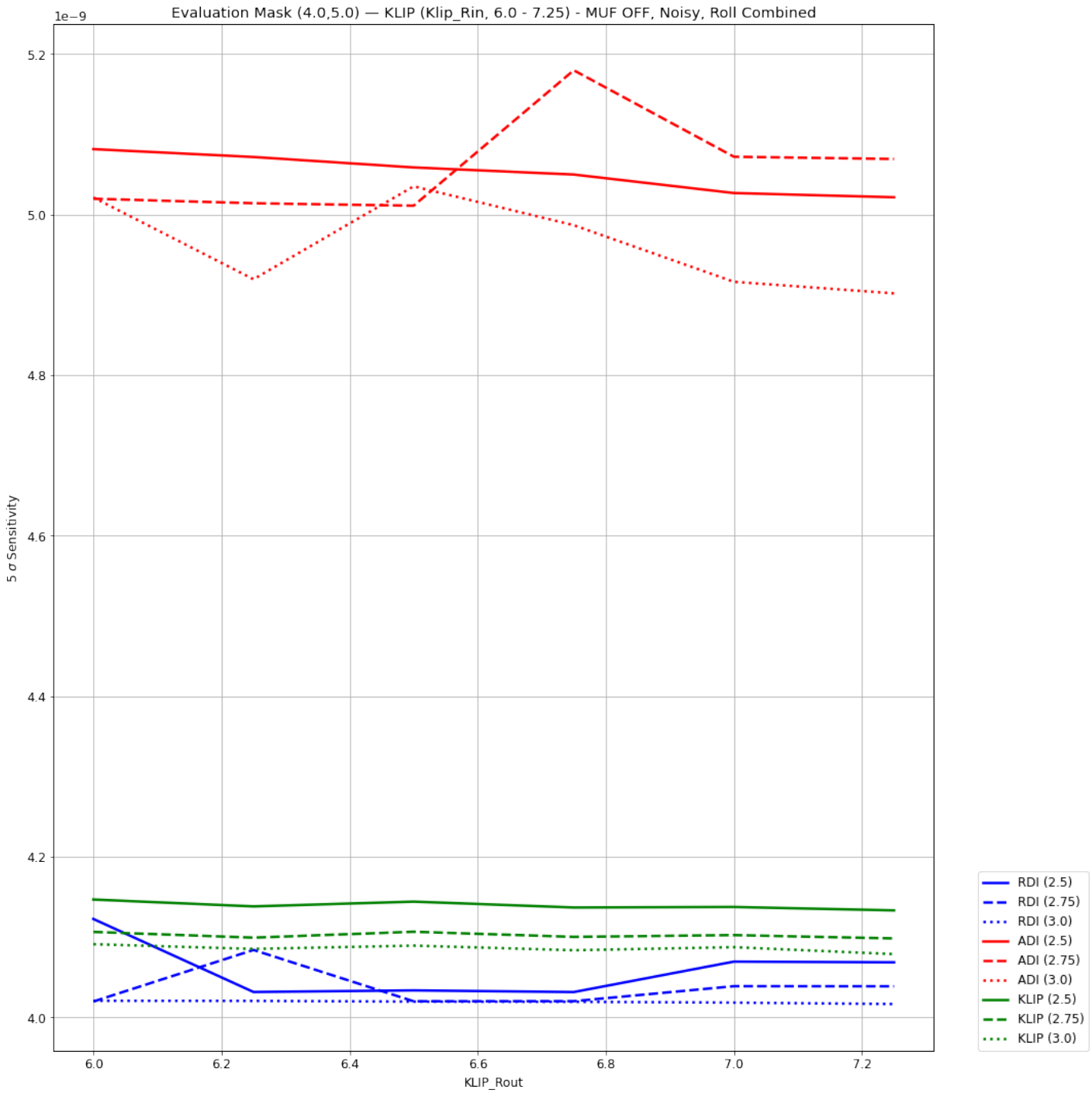

Figure 19: This graph uses an evaluation mask of 4 — 5 λ/D for the MUF off, noisy dataset. The graph shows the relationship between the increase of the outer angle of the KLIP mask (x-axis), and the contrast calculated for respective post-processing technique (y-axis, 5 σ sensitivity). The different colors of each line are a different post-processing technique, and the shape of the lines are the different inner-working angle of the KLIP mask.

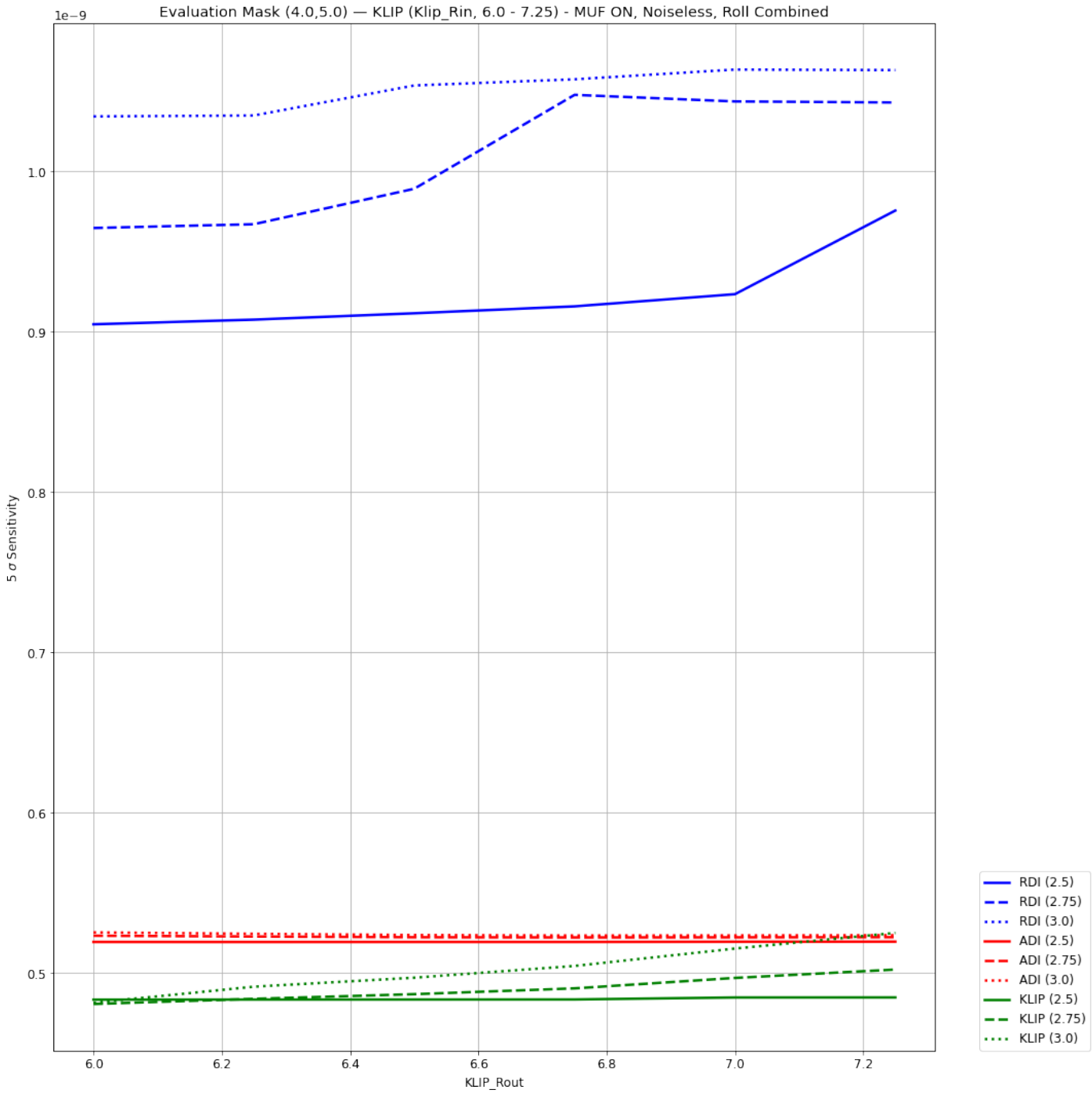

Figure 20: This graph uses an evaluation mask of 4 — 5 λ/D for the MUF on, noiseless dataset. The graph shows the relationship between the increase of the outer angle of the KLIP mask (x-axis), and the contrast calculated for respective post-processing technique (y-axis, 5 σ sensitivity). The different colors of each line are a different post-processing technique, and the shape of the lines are the different inner-working angle of the KLIP mask.

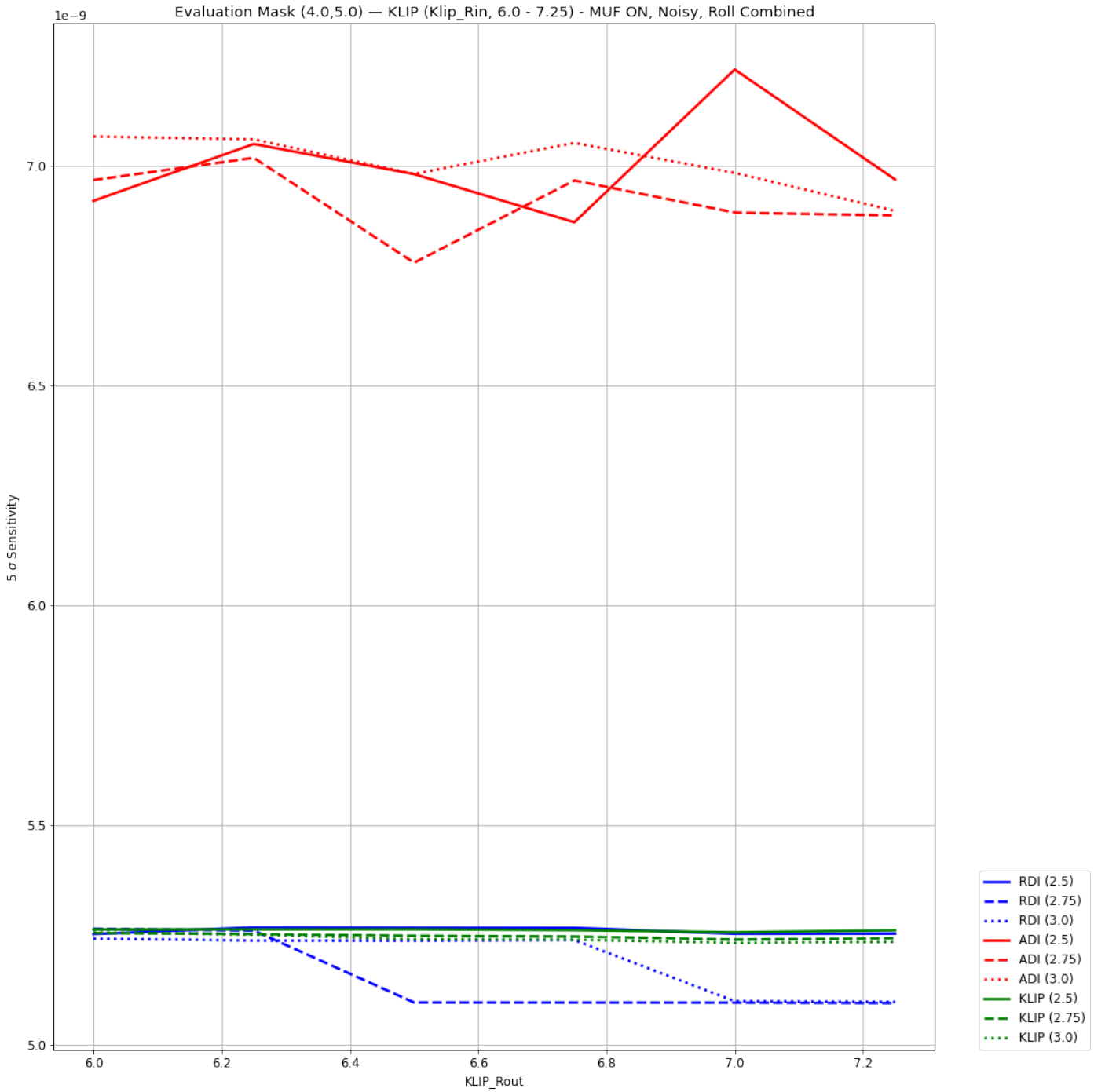

Figure 21: This graph uses an evaluation mask of 4 — 5 λ/D for the MUF on, noisy dataset. The graph shows the relationship between the increase of the outer angle of the KLIP mask (x-axis), and the contrast calculated for respective post-processing technique (y-axis, 5 σ sensitivity). The different colors of each line are a different post-processing technique, and the shape of the lines are the different inner-working angle of the KLIP mask.

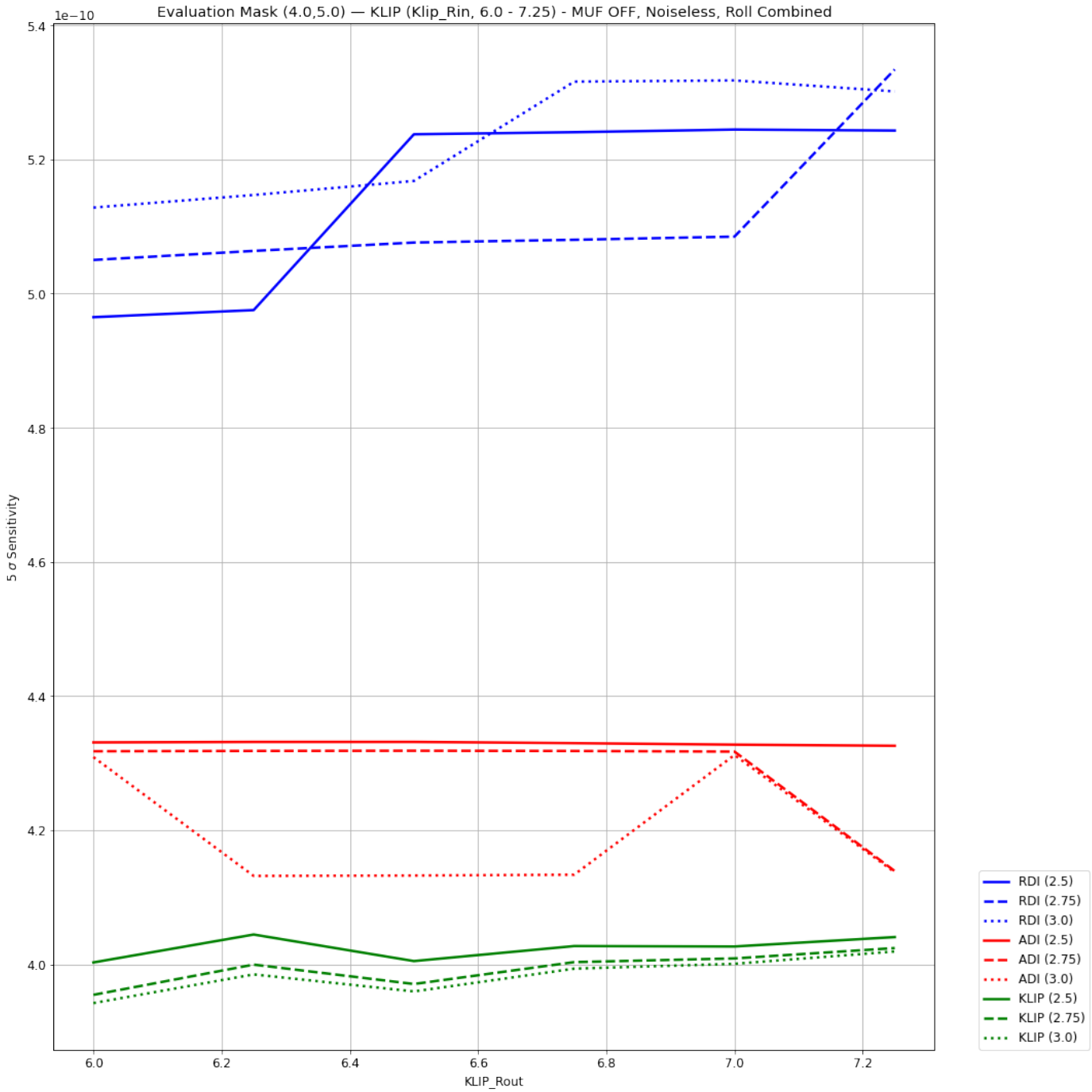

Figure 22: This graph uses an evaluation mask of 4 — 5 λ/D for the MUF off, noiseless dataset. The graph shows the relationship between the increase of the outer angle of the KLIP mask (x-axis), and the contrast calculated for respective post-processing technique (y-axis, 5 σ sensitivity). The different colors of each line are a different post-processing technique, and the shape of the lines are the different inner-working angle of the KLIP mask.

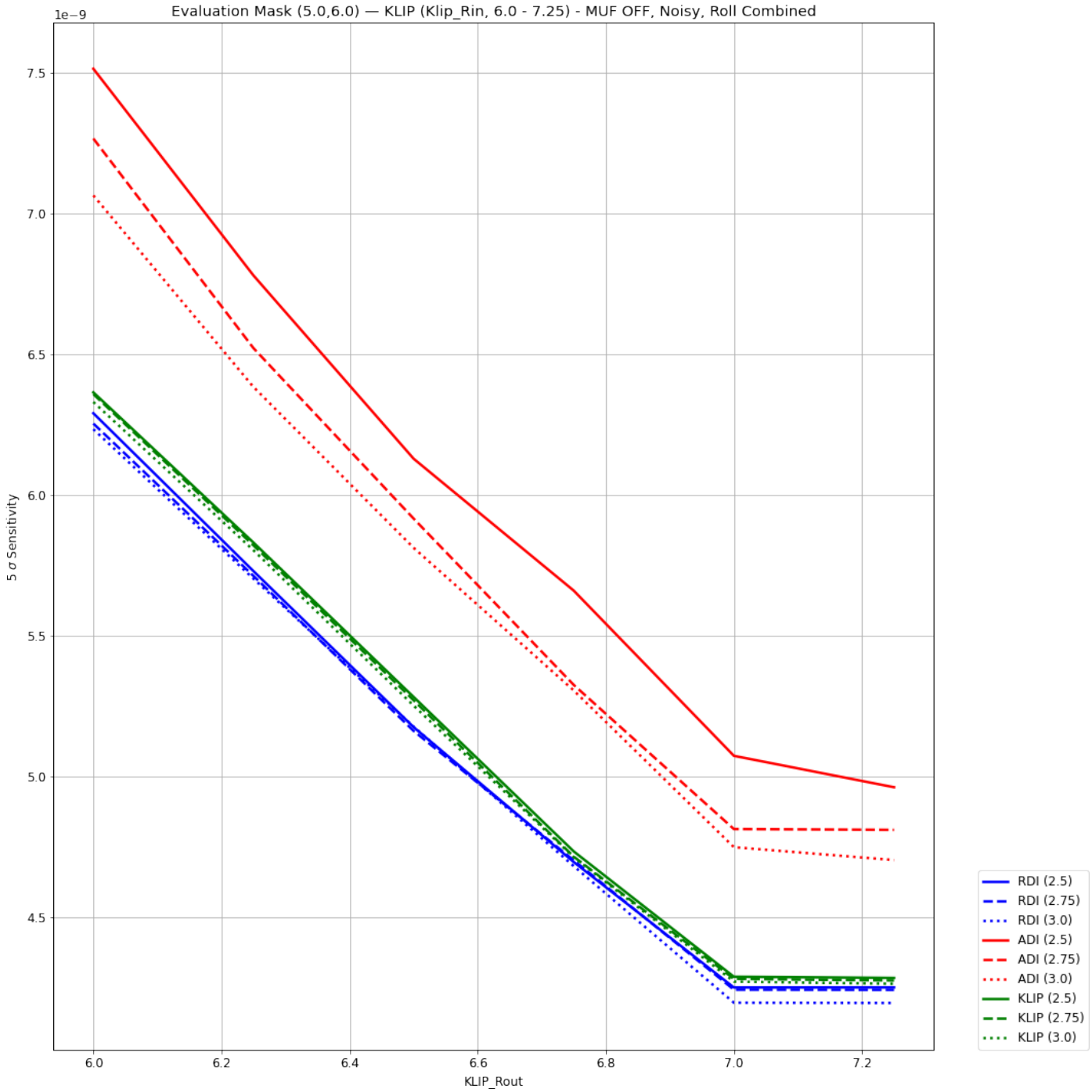

Figure 23: This graph uses an evaluation mask of 5 — 6 λ/D for the MUF off, noisy dataset. The graph shows the relationship between the increase of the outer angle of the KLIP mask (x-axis), and the contrast calculated for respective post-processing technique (y-axis, 5 σ sensitivity). The different colors of each line are a different post-processing technique, and the shape of the lines are the different inner-working angle of the KLIP mask.

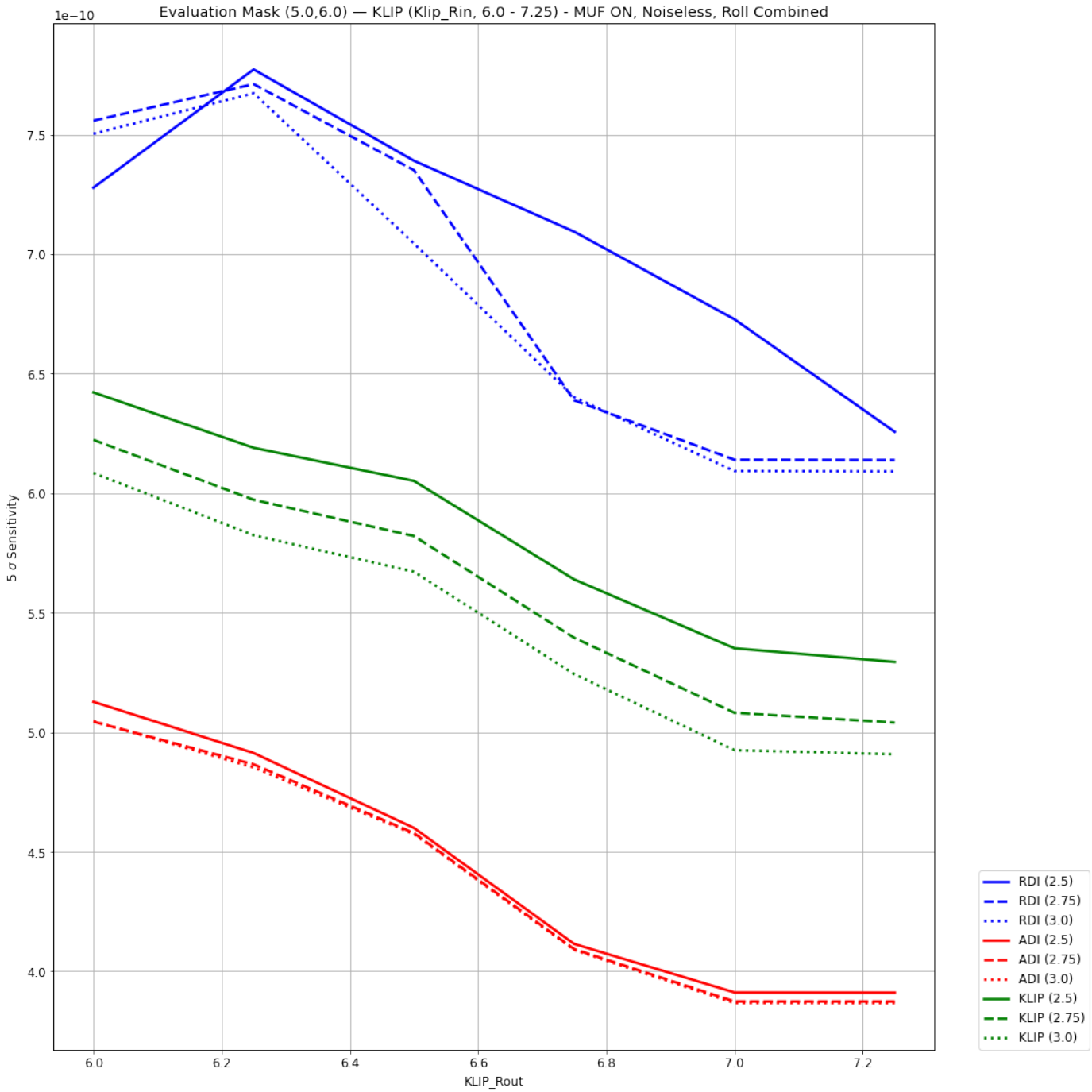

Figure 24: This graph uses an evaluation mask of $5 — 6\ \lambda/D$ for the MUF on, noiseless dataset. The graph shows the relationship between the increase of the outer angle of the KLIP mask (x-axis), and the contrast calculated for respective post-processing technique (y-axis, 5 σ sensitivity). The different colors of each line are a different post-processing technique, and the shape of the lines are the different inner-working angle of the KLIP mask.

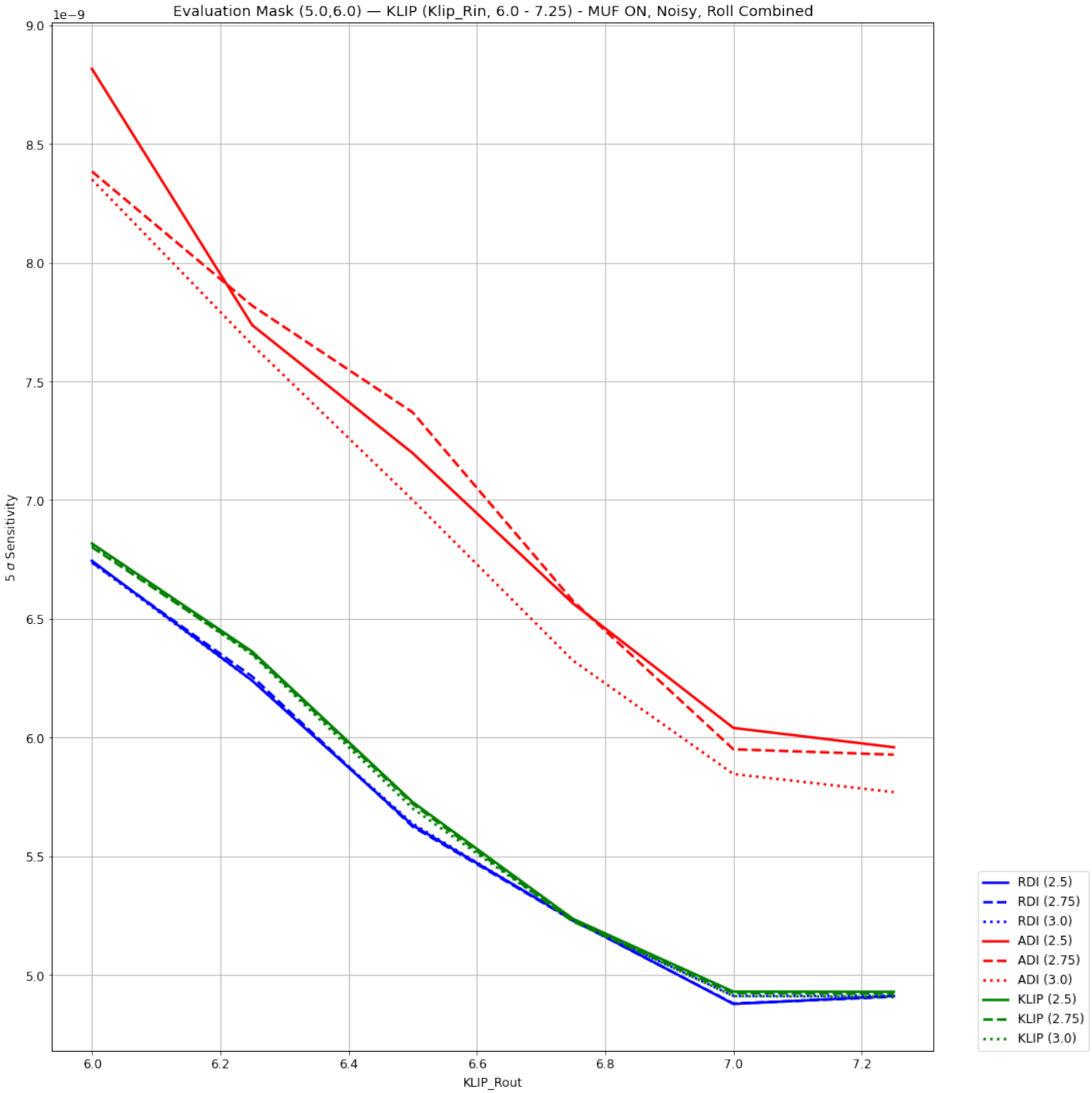

Figure 25: This graph uses an evaluation mask of 5 — 6 λ/D for the MUF on, noisy dataset. The graph shows the relationship between the increase of the outer angle of the KLIP mask (x-axis), and the contrast calculated for respective post-processing technique (y-axis, 5 σ sensitivity). The different colors of each line are a different post-processing technique, and the shape of the lines are the different inner-working angle of the KLIP mask.

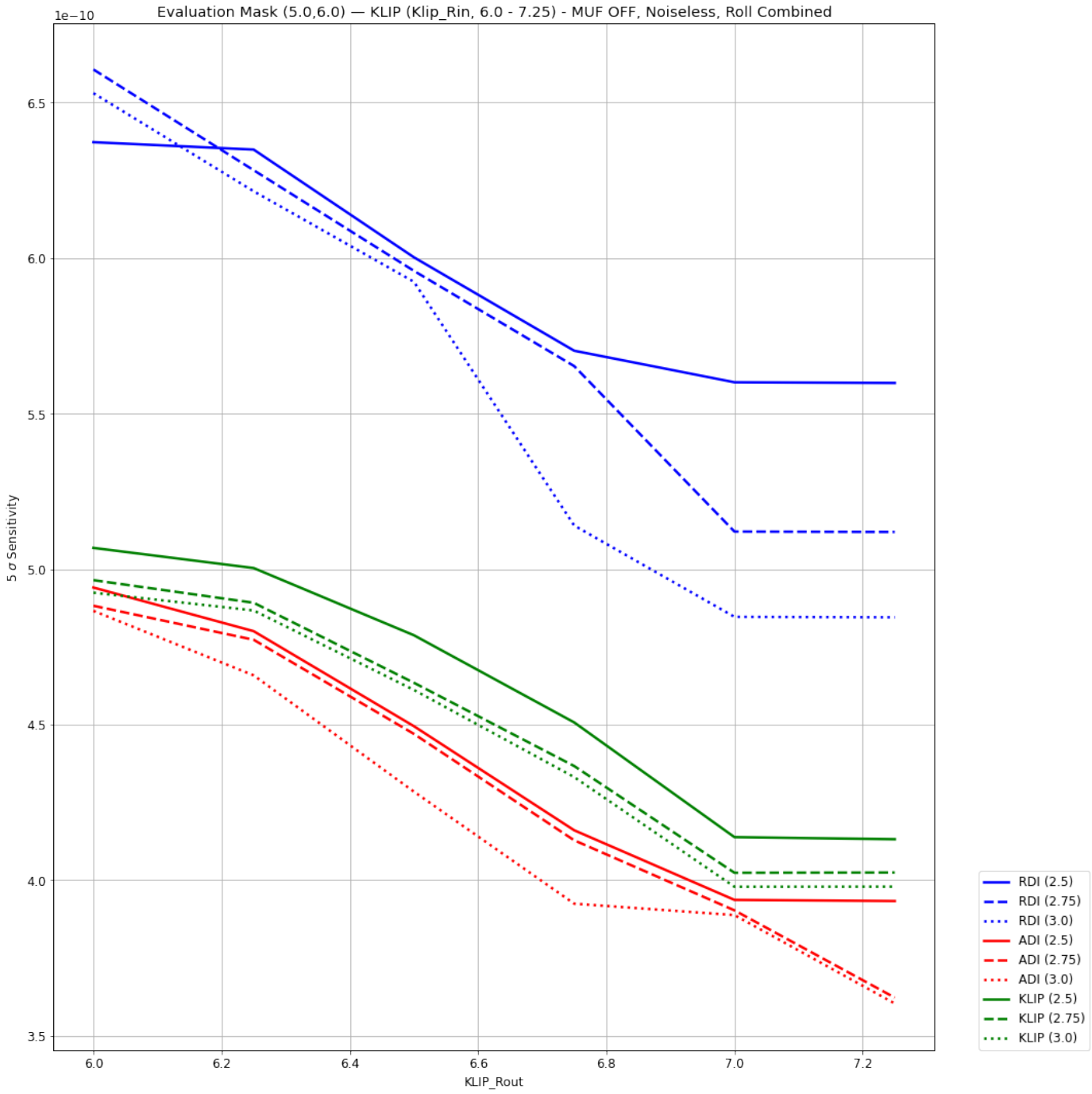

Figure 26: This graph uses an evaluation mask of 5 — 6 λ/D for the MUF off, noiseless dataset. The graph shows the relationship between the increase of the outer angle of the KLIP mask (x-axis), and the contrast calculated for respective post-processing technique (y-axis, 5 σ sensitivity). The different colors of each line are a different post-processing technique, and the shape of the lines are the different inner-working angle of the KLIP mask.